Y. Q. Yan, T. B. Smith, J. Li, J. Y. Lin, and H. X. Jiang

COLLECTIONS

Paper published as part of the special topic on Chemical Physics, Energy, Fluids and Plasmas, Materials Science and Mathematical Physics

View Online   Export Citation   CrossMark

Erbium energy levels in GaN grown by hydride vapor phase epitaxy

Y. Q. Yan, [ID] T. B. Smith, J. Li, [ID] J. Y. Lin, [ID] and H. X. Jiang[a) [ID]

AFFILIATIONS

Department of Electrical and Computer Engineering, Texas Tech University, Lubbock, Texas 79409, USA
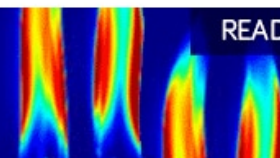
[a)]Author to whom correspondence should be addressed: hx.jiang@ttu.edu

ABSTRACT

Erbium doped GaN (Er:GaN) is a promising candidate as a novel gain medium for solid-state high energy lasers (HELs) due to its superior physical properties over a synthetic garnet such as Nd:YAG. Er:GaN emits in the 1.5 μm region, which is retina-safe and has a high transmission in the air. We report photoluminescence (PL) studies performed on Er:GaN epilayers synthesized by the hydride vapor phase epitaxy (HVPE) technique. The room temperature PL spectra of HVPE grown Er:GaN epilayers resolved as many as 11 and seven emission lines in the 1.5 μm and 1.0 μm wavelength regions, respectively, corresponding to the intra-4f shell transitions between Stark levels from the first ($^4I_{13/2}$) and the second ($^4I_{11/2}$) excited states to the ground state ($^4I_{15/2}$) of Er^{3+} in GaN. The observed peak positions of these transitions enabled the construction of the detailed energy levels in Er:GaN. The results agree well with those of the calculation based on a crystal field analysis. Precise determination of the detailed energy levels of the Stark levels in the $^4I_{11/2}$, $^4I_{13/2}$, and $^4I_{15/5}$ states is critically important for the realization of HELs based on Er:GaN.

INTRODUCTION

An optical gain medium is the heart of solid-state high energy laser (HEL) systems, which have been investigated for decades due to their numerous applications in communication, defense, manufacturing, and medicine.[1] The most common gain material for solid-state HELs today is the synthetic garnet such as YAG doped with neodymium (Nd:YAG) emitting at 1.06 μm. Erbium doped GaN (Er:GaN) is a promising new candidate as a gain medium for HELs operating at 1.5 μm,[2–5] as the Er^{3+} ion in GaN has an allowable intra-4f shell transition from its first excited state ($^4I_{13/2}$) to the ground state ($^4I_{15/2}$) that lies in the 1.5 μm spectral region, which has a high thermal stability[3,6,7] and high transmission in the air[8] and is retina-safe.[9] Furthermore, GaN as a host material has outstanding thermal, mechanical, and optical properties over YAG. Compared to YAG, GaN has a much higher thermal conductivity of $\kappa \approx 253$ W/m K ($\kappa = 14$ W/m K for YAG) and a smaller thermal expansion coefficient of $\alpha \approx 3.53 \times 10^{-6}\,^\circ C^{-1}$ ($\alpha \approx 7 \times 10^{-6}\,^\circ C^{-1}$ for YAG) at room temperature.[10–13]

Metal-organic chemical vapor deposition (MOCVD) and molecular beam epitaxy (MBE) are the two major techniques

used for the growth of Er:GaN epitaxial thin films with a typical thickness of less than 5 μm and low growth rate of about 1 μm/h.[7,14–34] For HEL applications, Er:GaN with large thicknesses and, hence, high growth rates is needed. Er:GaN bulk crystals have been synthesized recently via the hydride vapor phase epitaxy (HVPE) technique at high growth rates (up to ~200 μm/h).[3–5] Although the basic properties of Er doped GaN thin films grown by MOCVD and MBE have been widely reported,[7,14–34] studies on the optical properties of Er:GaN grown by HVPE have been limited.[2–5]

For HEL applications, the energy levels of the Stark levels of $^4I_{11/2}$ (absorption) and $^4I_{13/2}$ (emission) determine pumping and lasing wavelengths. Moreover, the energy levels of these manifolds also determine the important parameters of Er:GaN as a gain medium, including the population distribution of the excited states of Er among different Stark levels, emission intensities, gain coefficient, and lasing threshold power density. We report here HVPE growth and photoluminescence (PL) emission spectroscopy studies of Er:GaN epilayers and the determination of detailed energy levels of the second excited state ($^4I_{11/2}$), the first excited state ($^4I_{13/2}$), and the ground state ($^4I_{15/2}$) of Er^{3+} in GaN, which are critical for
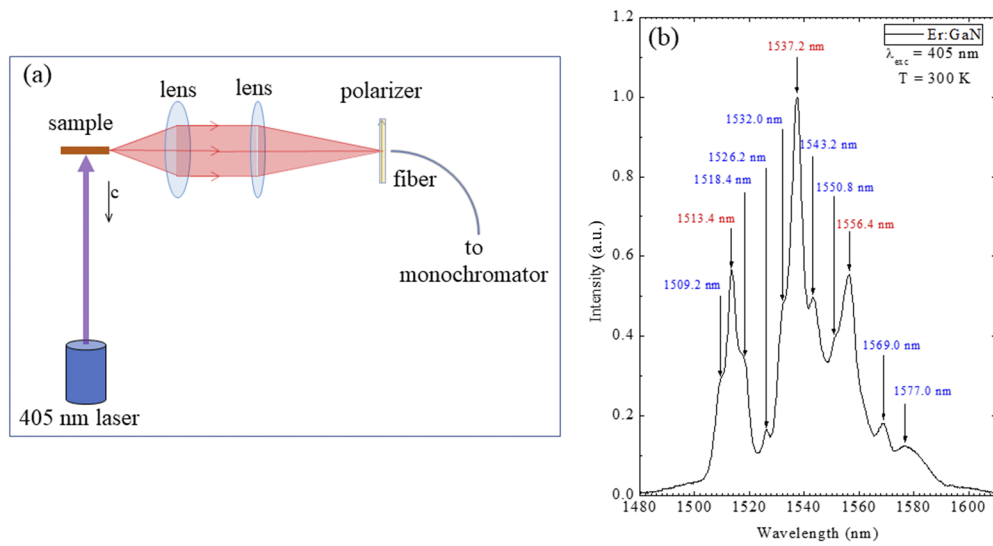
FIG. 1. (a) Schematic setup of PL measurements. To record polarization-resolved PL spectra, two lenses and a polarizer were added in between the Er:GaN sample and the monochromator. (b) Room temperature PL emission spectrum of an as-grown Er:GaN sample under photoexcitation by a 405 nm LD, measured from 1480 nm to 1610 nm. The peak wavelengths at 1513.4 nm, 1537.2 nm, and 1556.4 nm highlighted in red color are the dominant transitions with the highest emission intensities.
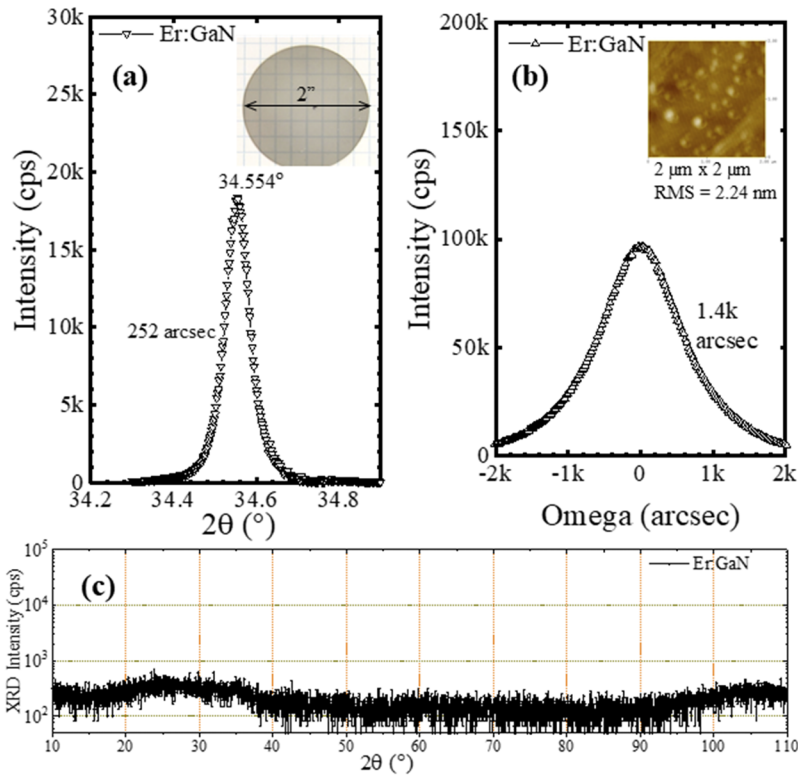
FIG. 2. X-ray diffraction (XRD) spectra of the (a) θ–2θ scan, (b) rocking curve of the (0002) reflection peak, and (c) polycrystal scan (5° off with respect to the c-axis of GaN) of an as-grown Er:GaN sample. The inset of (a) is an optical image of an as-grown Er:GaN wafer of 2-in. in diameter grown by HVPE. The inset of (b) is an atomic force microscopy (AFM) surface morphology of an as-grown Er:GaN sample over a scan area of 2×2 μm^2 revealing a surface roughness rms value of 2.2 nm.

basic understanding as well as practical applications of Er:GaN as an emerging optical gain material.

EXPERIMENTS

Prior to the growth of Er:GaN, a 3 μm GaN epilayer was first deposited on a c-plane sapphire substrate of 2 in. in diameter by MOCVD to serve as a template for the subsequent growth of Er:GaN by the HVPE method. The HVPE system contains Ga and Er metal sources with purities of 99.9999% and 99.9%, respectively. H_2 gas was used as a carrier gas, and the growth temperature was 1120 $°$C. X-ray diffraction (XRD) measurements were performed to determine the crystalline quality of the as-grown Er:GaN samples.

PL spectra were measured at room temperature using a laser diode (LD) with a lasing wavelength of λ_{exc} = 405 nm as an excitation source to provide the band edge excitation. The PL emission was collected using a fiber coupled with a monochromator and an InGaAs detector providing an overall spectral resolution of 0.2 nm. The propagation direction of the excitation light, k_{exc}, was always parallel to the sample's c-axis, whereas that of the PL emission, k_{emi}, was perpendicular to the sample's c-axis. The excitation power intensity dependence of PL spectra was measured by controlling the lasing power of the LD by changing its operating current. Polarization-resolved PL emission spectra were measured by placing a polarizer in between the Er:GaN sample and the monochromator in such a way that transverse magnetic (TM) and transverse electric (TE) emission modes can be changed by controlling the direction of the polarizer. There were also two optical lenses in the setup. A collimating lens collects the PL emission from the sample and outputs a parallel beam, whereas a second lens focuses the parallel beam to the fiber, as schematically shown in Fig. 1(a). A typical room temperature PL spectrum of the Er:GaN epilayer grown by HVPE measured in the 1.5 μm region is shown in Fig. 1(b), which exhibits three dominant emission peaks at 1513.4 nm, 1537.2 nm, and 1556.4 nm (marked in red color).

RESULTS

The inset of Fig. 2(a) shows the optical image of an as-grown Er:GaN wafer of 2-in. in diameter with high transparency and a smooth surface. The thickness of the Er:GaN layer is 12 μm with an Er concentration of 3 × 10^{19}/cm^3, based on reference samples measured by secondary ion mass spectrometry. An atomic force microscopy (AFM) image of this as-grown Er:GaN sample is shown in the inset of Fig. 2(b), which reveals an AFM surface root-mean-square (rms) roughness of 2.2 nm over a scan area of 2 × 2 μm^2. The θ–2θ scan of x-ray diffraction (XRD) results of this as-grown Er:GaN sample is shown in Fig. 2(a), exhibiting a high intensity and narrow full-width at half-maximum (FWHM) of 252 arcsec. The observed position of the (0002) reflection peak at 34.554$°$ is close to the ideal (0002) peak position of strain free GaN at 34.569$°$, but signifying the presence of small strain in Er:GaN. The XRD rocking curve of the (0002) peak is shown in Fig. 2(b) and has a FWHM of 1400 arcsec, indicating that Er:GaN grown by HVPE has a reasonable crystalline quality. Figure 2(c) plots the θ–2θ scan from 10$°$ to 110$°$

measured at an orientation of 5$°$ off with respect to the c-axis of Er:GaN, showing no observable peaks. The results indicate that no polycrystalline structures are present and the as-grown Er:GaN film is a single crystal.

Figure 1(b) shows the room temperature PL spectrum measured in the range of 1480 nm–1610 nm, which covers transitions between different Stark levels in the first excited state ($^4I_{13/2}$) and the ground state ($^4I_{15/2}$) of Er^{3+} ions. The previous room temperature PL spectra of Er:GaN epilayers typically exhibit only five or six emission lines in this spectral range,[2–5,29–34] while 11 peaks in total were clearly resolved in the spectrum of HVPE grown Er:GaN, as shown in Fig. 1(b). The results are a clear indication that Er:GaN materials produced by HVPE in the present work possess a very high optical quality.

The room temperature PL spectrum measured between 970 nm and 1020 nm is shown in Fig. 3, which covers the transitions between different Stark levels in the second excited state ($^4I_{11/2}$) and the ground state ($^4I_{15/2}$) of Er^{3+} ions. In total, seven emission peaks were clearly resolved in this spectral region with peak positions indicated in this figure. The strongest emission line is at 1.0 μm. It is interesting to note that the peak position of this 1.0 μm emission line

FIG. 3. Room temperature PL emission spectrum of an as-grown Er:GaN sample under an excitation of a 405 nm LD, measured from 970 nm to 1020 nm. The wavelengths highlighted in red color are the dominant transitions with highest emission intensities.
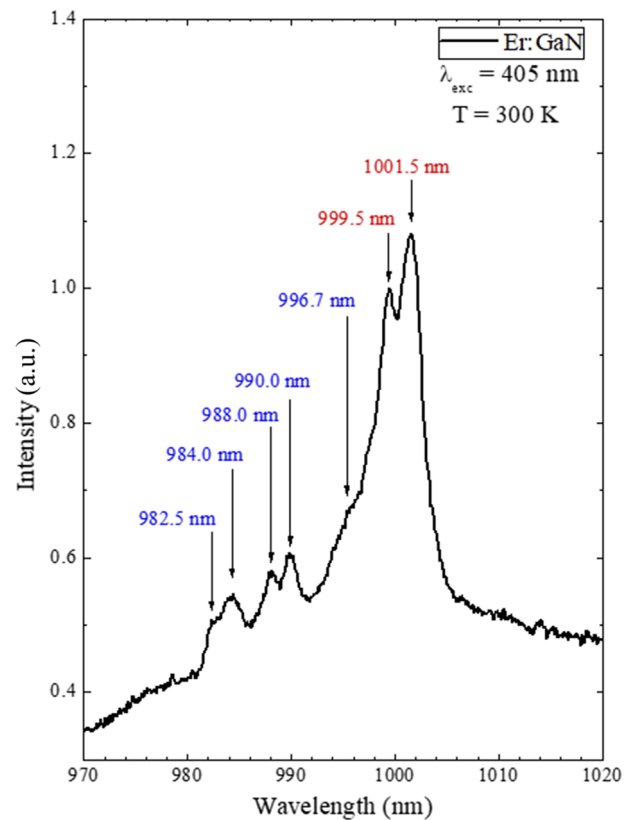
observed in Er:GaN slightly differs from the corresponding emission line in Er:YAG at 0.98 μm.[35] We believe that the difference of the detailed crystal fields around Er atoms in GaN and YAG is most likely responsible for this difference. However, this slight difference in the transition peak position has a large consequence in the selection of optical pumping sources, i.e., a pumping wavelength of 1.0 μm should be employed for Er:GaN instead of the more common pump wavelength at 0.98 μm for Er doped YAG. Again, the emission peaks in this spectrum show high intensities with narrow linewidths.

The PL emission intensities, I_{emi}, of the dominant emission lines at 1513.4 nm (red triangles), 1537.2 nm (blue squares), and 1556.4 nm (green circles) were also measured at varying excitation intensities, I_{exc}, and the results are shown in Fig. 4. We noted that the emission intensities exhibit rapid increases initially and saturate with a further increase in the excitation intensity. The curves in Fig. 4 are the least squares fits of data with the following relationship:

$$I_{emi} = A \cdot I_{exc}{}^{\alpha}, \tag{1}$$

where A is a constant and α describes a power-law dependence of I_{emi} vs I_{exc}. The fitted values of A for emission wavelengths at 1513.4 nm, 1537.2 nm, and 1556.4 nm are 1.85×10^{-2}, 3.37×10^{-2}, and 1.86×10^{-2}, respectively. It is interesting to note that the fitted values of parameter A are very close for the emission lines at 1513.4 nm and 1556.4 nm. The exponent α of the power-law dependence for the emission lines at 1513.4 nm, 1537.2 nm, and 1556.4 nm is 0.53, 0.53, and 0.54, respectively, which are all close to 0.5, meaning that I_{emi} exhibits a nearly square root power dependence on I_{exc}. A similar behavior was observed previously in TiO_2 nanocrystals[36] and SiO_2 nanocrystals.[37]

The polarization-resolved PL spectra measured from 1480 nm to 1610 nm for both the TM (blue spectrum, **E//c**) and TE (red spectrum, **E⊥c**) emission modes are shown in Fig. 5. In obtaining these results, the excitation laser was unpolarized. Figure 5 shows that the emission intensity of the TE (**E⊥c**) mode is 25% lower than that of the TM (**E//c**) mode. The measured results are consistent with the higher excitation/absorption efficiency of the TM mode in Er:GaN. This can be attributed to a higher excitation efficiency of the TM mode due to the presence of the spontaneous polarization field, which acts along the direction of the c-axis of GaN.[38]
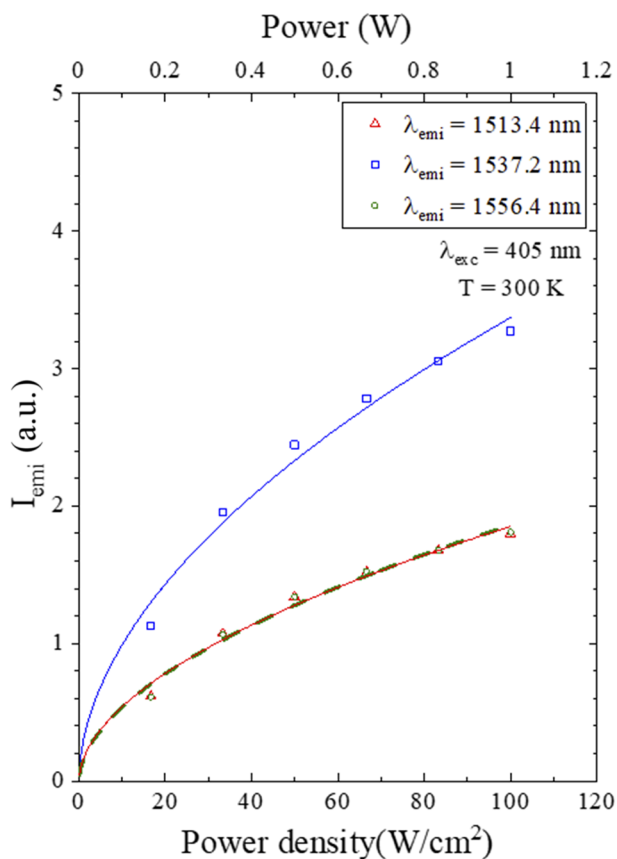

FIG. 4. PL emission intensities as functions of excitation intensity measured for the three dominant emission lines with peak positions at 1513.4 nm (red triangles), 1537.2 nm (blue squares), and 1556.4 nm (green circles). The solid and dashed curves are the least squares fits with Eq. (1) of data measured at 1513.4 nm (red solid curve), 1537.2 nm (blue solid curve), and 1556.4 nm (green dashed curve).
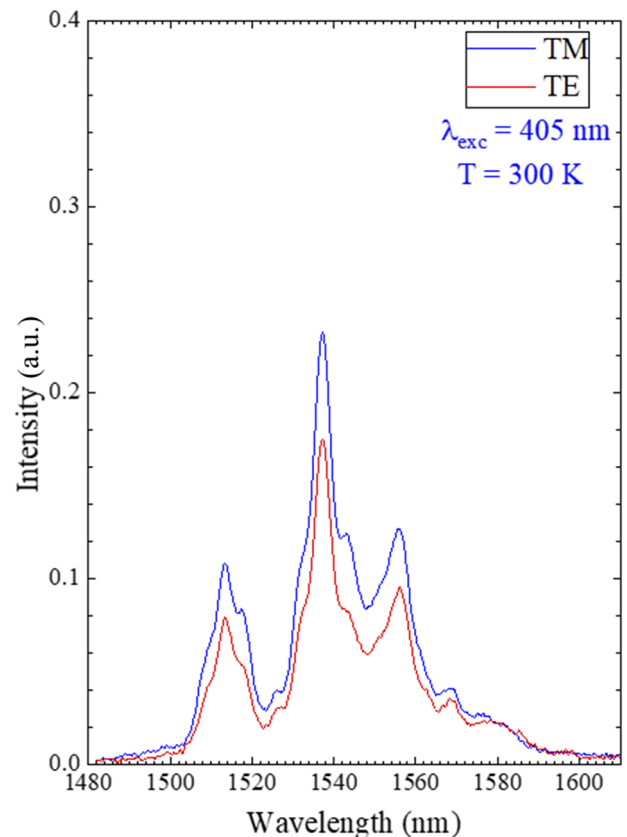

FIG. 5. Room temperature polarization-resolved PL spectra of an as-grown Er:GaN sample under the excitation of a 405 nm LD measured in the TM (blue spectrum) and TE (red spectrum) modes from 1480 nm to 1610 nm.

ANALYSIS

The fine features of PL spectra shown in Figs. 1(b) and 3 allow us to extract a large amount of useful information, including the detailed energy level diagram of the Stark levels in the $^4I_{11/2}$, $^4I_{13/2}$, and $^4I_{15/2}$ manifolds. The Stark levels of the ground state ($^4I_{15/2}$), the first excited state ($^4I_{13/2}$), and the second excited state ($^4I_{11/2}$) were deduced from the observed peak positions in the PL spectra shown in Figs. 1(b) and 3 and are presented in Table I. Table I also includes all possible transition lines from the Stark levels in the excited states to the Stark levels of the ground state. For comparison, the calculated energy levels (in units of cm^{-1}) of Er^{3+} ions in wurtzite GaN based on a crystal field analysis are also included in Table I.[26] The top row in Table I indicates the eight Stark levels in the $^4I_{15/2}$

manifold, whereas the top and bottom of the left columns of Table I list the seven Stark levels of the first excited state ($^4I_{13/2}$) and the six Stark levels of the second excited state ($^4I_{11/2}$), respectively. The calculated energy levels in these cells are indicated by the black color, whereas the peak positions observed from Figs. 1(b) and 3 are indicated in green color in the same cells. The corresponding calculated emission wavelengths (in units of nm) involving the transitions from the Stark levels of the upper states ($^4I_{13/2}$ and $^4I_{11/2}$) listed in the left column to the Stark levels of the ground state ($^4I_{15/2}$) listed in the top row are marked in black. The numerical values in blue and red colors in each cell in Table I correspond to the peak positions of the observed emission lines from Figs. 1(b) and 3 in the unit of nm. The wavelengths indicated in red color are the dominant transitions in the PL spectra with the highest intensities, as

TABLE I. The energy levels (in cm^{-1}) of the manifolds in the ground state ($^4I_{15/2}$), the first excited state ($^4I_{13/2}$), and the second excited state ($^4I_{11/2}$) extracted from the observed peak positions in the PL emission spectra of Figs. 1(b) and 3 (bold fonts). The energy levels obtained from calculation (normal fonts) based on a crystal field analysis are included for comparison. The peak positions (in nm) observed from Figs. 1(b) and 3 are indicated in italic (with highest intensities) and bold italic (with lower intensities), whereas the calculated wavelength of possible transitions (Ref. 26) is indicated by the normal fonts in the same cells.

(nm)	$^4I_{15/2}$ (cm^{-1})	4.7 **4.7**	10.2 **10.2**	39.1 **39.1**	111.0 **111.0**	150.8 **156.2**	166.3 **168.9**	184.3 **187.9**	195.5 **196.2**
$^4I_{13/2}$ (cm^{-1}) (1503 nm–1585 nm)	6510.1 **6510.1**	1537.2 1537.2	1538.5	1545.4	1562.7	1572.5	1576.3 **1577.0**	1580.8	1583.6
	6515.5 **6515.5**	1535.9	1537.2 1537.2	1544.1	1561.4	1571.2	1575.0	1579.5	1582.3
	6543.2 **6542.4**	1529.4	1530.7	1537.5	1554.7	1564.4	1568.2 **1569.0**	1572.6	1575.4
	6602.1 **6596.1**	1515.7	1517.0 **1518.4**	1523.7	1540.6	1550.1	1553.8	1558.2	1560.9
	6613.3 **6613.0**	1513.2 1513.4	1514.4	1521.1	1537.9	1547.4	1551.1	1555.5 **1556.4**	1558.2
	6633.8 **6636.2**	1508.5	1509.8 **1509.2**	1516.4	1533.1 **1532.0**	1542.5 **1543.2**	1546.2	1550.5 **1550.8**	1553.2
	6651.6 **6663.2**	1504.5	1505.7	1512.3	1528.9 **1526.2**	1538.3	1541.9	1546.2	1548.9
$^4I_{11/2}$ (cm^{-1}) (980 nm–1004 nm)	10 137.0 **10 141.2**	986.9	987.5	990.3	997.4	1001.4 1001.5	1002.9	1004.8	1005.9
	10 150.2 **10 153.9**	985.7	986.2	989.0	996.1	1000.1	1001.6 1001.5	1003.4	1004.6
	10 165.2 **10 160.5**	984.2	984.7	987.5 **988.0**	994.6	998.6	1000.1	1001.9	1003.0
	10 186.9 **10 188.3**	982.1	982.6 **982.5**	985.4	992.5	996.4	997.9	999.7	1000.9
	10 201.2 **10 201.2**	980.7	981.3	984.0 **984.0**	991.1	995.0	996.5 **996.7**	998.3	999.4 **999.5**
	10 212.2 **10 212.2**	979.7	980.2	983.0	990.0 **990.0**	993.9	995.4	997.2	998.3

they are highlighted in red color in Figs. 1(b) and 3, which correspond to emission wavelengths with the largest emission cross sections. The wavelengths highlighted in blue color are the PL emission peaks with lower intensities. For each emission peak wavelength in Figs. 1(b) and 3, the closest value from the calculated wavelength in Table I was determined and used to construct the energy levels of Er in GaN. Among them, the emission peak at 1537.2 nm has two exact matches in Table I at 1537.2 nm. For the emission wavelength at 1001.5 nm, because the calculated wavelengths of 1001.4 nm and 1001.6 nm are both within 0.1 nm from the measured wavelength, hence, they were both chosen as the possible transition lines.

　　Table II compares the experimental and calculated energy levels of the Stark levels in $^4I_{15/2}$, $^4I_{13/2}$, and $^4I_{11/2}$ states. The values for E_{calc} were based on the calculation for wurtzite GaN with C_{3v} symmetry.[26] The values for $E_{expt.}(MOCVD)$ represent the measured energy levels obtained from Er:GaN epilayers previously grown by MOCVD and those of $E_{expt.}(HVPE)$ are the measured energy levels of the present work. The energy differences between $E_{expt.}(MOCVD)$, $E_{expt.}(HVPE)$ and E_{calc} are denoted by Δ_1 and Δ_2, where $\Delta_1 = E_{expt.}(MOCVD) - E_{calc}$ and $\Delta_2 = E_{expt.}(HVPE) - E_{calc}$. The results in Table II clearly demonstrate that the values of Δ_2 are much smaller than those of Δ_1, demonstrating that the experimental results obtained in this work agree much better with the calculation results in comparison with earlier data from $E_{expt.}(MOCVD)$.[26] It is worth mentioning that the PL spectra of $E_{expt.}(MOCVD)$ were

measured at low temperatures (6 K) with the hope to provide improved spectral resolution and emission intensities,[26] whereas the PL spectra presented here were all measured at room temperature. The rich spectral features resolved in the room temperature PL spectra shown in Figs. 1(b) and 3 enable us to construct a detailed energy level diagram of the Stark levels in the $^4I_{15/2}$, $^4I_{13/2}$, and $^4I_{11/2}$ manifolds of Er^{3+} in GaN. From Table II, $E_{expt.}(MOCVD)$ did not fit well the sixth Stark level of the ground state ($^4I_{15/2}$) and the fourth to seventh Stark levels of the first excited state ($^4I_{13/2}$). In comparison, the present results agree very well with all the calculated energy levels of different Stark levels in the $^4I_{11/2}$, $^4I_{13/2}$, and $^4I_{15/2}$ states. A direct quantitative comparison for the energy level differences between the measured and calculated energy levels can be made by evaluating the standard deviation,

$$\sigma = \sqrt{\sum_{i=1,...,N_E} \left(E_i(calc) - E_i(exp)\right)^2 / N_E}, \quad (2)$$

where $E_i(cal.)$ and $E_i(expt.)$ are the calculated and measured energy levels in Table II, respectively, and N_E denotes the numbers of experimentally measured energy levels fitted. The calculation yields $\sigma_1 = 9.1\ cm^{-1}$ for $E_{expt.}(MOCVD)$ and $\sigma_2 = 3.7\ cm^{-1}$ for the present results, $E_{expt.}(HVPE)$. The much-reduced value of σ_2 over σ_1 again confirms a significant improvement in the accuracy of the present results over those of the earlier measurements of MOCVD samples.[26]

TABLE II. Comparison between the experimentally measured [$E_{expt.}(MOCVD)$ and $E_{expt.}(HVPE)$] and calculated (E_{calc}) energy levels of the manifolds in $^4I_{15/2}$, $^4I_{13/2}$, and $^4I_{11/2}$ states of Er^{3+} ions in GaN. The values for E_{calc} were based on the calculation for wurtzite GaN with C_{3v} symmetry (Ref. 26). The values of $E_{expt.}(MOCVD)$ were extracted from the low temperature PL spectra of Er:GaN epilayers grown by MOCVD, and the values of $E_{expt.}(HVPE)$ were extracted from the room temperature PL spectra of Figs. 1(b) and 3 of the present work.

(cm^{-1})	$E_{expt.}(MOCVD)$	$E_{expt.}(HVPE)$	E_{calc}	$\Delta_1 = E_{expt.}(MOCVD) - E_{calc}$	$\Delta_2 = E_{expt.}(HVPE) - E_{calc}$
	0.0	4.7	4.7	−4.7	0
	4.4	10.2	10.2	−5.8	0
	32.0	39.1	39.1	−7.1	0
$^4I_{15/2}$	121.3	111.0	111.0	10.3	0
	158.6	156.2	150.8	7.8	5.4
	. . .	168.9	166.3	. . .	2.6
	189.0	187.9	184.3	4.7	3.6
	195.9	196.2	195.5	0.4	0.7
	6504.8	6510.1	6510.1	−5.3	0
	6511.8	6515.5	6515.5	−3.7	0
	6529.4	6542.4	6543.2	−13.8	−0.8
$^4I_{13/2}$	. . .	6596.1	6602.1	. . .	−6.0
	. . .	6613.0	6613.3	. . .	−0.3
	. . .	6636.2	6633.8	. . .	2.4
	. . .	6663.2	6651.6	. . .	11.6
	10 152.1	10 141.2	10 137.0	15.1	4.2
	10 168.8	10 153.9	10 150.2	18.6	3.7
$^4I_{11/2}$	10 173.2	10 160.5	10 165.2	8.0	−4.7
	10 186.6	10 188.3	10 186.9	−0.3	1.4
	10 190.6	10 201.2	10 201.2	−10.6	0
	10 205.1	10 212.2	10 212.2	−7.1	0

Achieving population inversion is a necessary condition for attaining lasing or gain in a gain medium. As such, understanding the Boltzmann population among different Stark levels in the $^4I_{11/2}$, $^4I_{13/2}$, and $^4I_{15/2}$ states is important. Figure 6 shows the constructed energy level diagram based on the results from Tables I and II and the corresponding Boltzmann populations, f_{li}, at room temperature, with l representing the l-th states and i representing the i-th Stark levels, which were calculated using

$$f_{li} = \frac{e^{-\frac{\Delta E_i}{kT}}}{\sum_{i=1}^{n} e^{-\frac{\Delta E_i}{kT}}} \; (l = 1, i = 1 \text{ to } 8 \text{ for } {}^4I_{15/2}, l = 2, i = 1 \text{ to } 7 \text{ for } {}^4I_{13/2}, l = 3, i = 1 \text{ to } 6 \text{ for } {}^4I_{11/2}), \quad (3)$$

where E_i represents the energy level of the i-th Stark level, k is the Boltzmann constant, and T is the temperature. Based on this constructed energy diagram, a quasi-four-level system can be achieved with the pumping wavelength at 1.0 μm, which has the highest
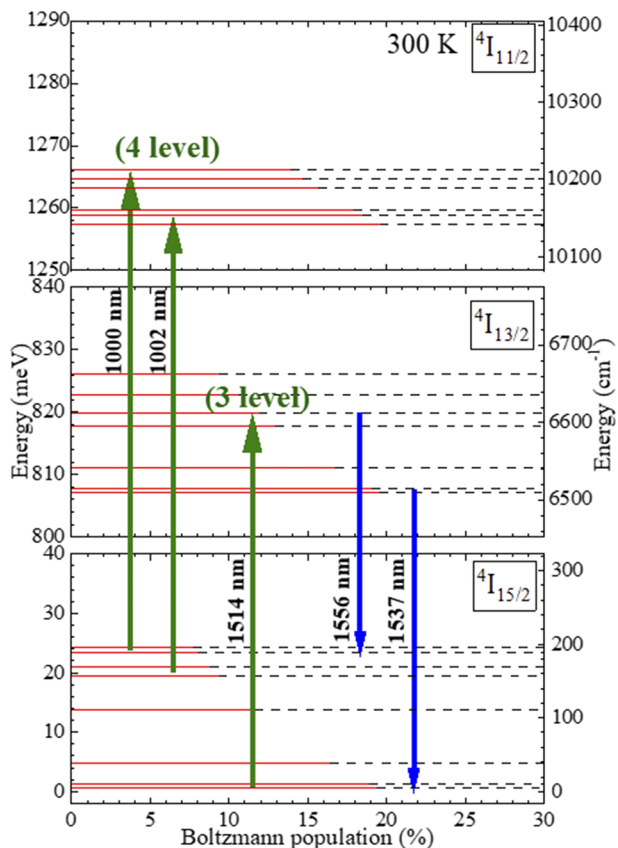

FIG. 6. Room temperature Stark energy level diagram constructed from the PL emission spectroscopy results of Figs. 1(b) and 3 and Tables I and II and the corresponding Boltzmann populations (red lines), including the detailed energy levels of manifolds in the $^4I_{11/2}$, $^4I_{13/2}$, and $^4I_{15/2}$ states of Er:GaN, which indicates that Er:GaN can be resonantly pumped at 1 μm or 1514 nm with the expected lasing wavelength occurring at 1537 nm or 1556 nm.

emission intensity as well as the highest absorption efficiency, as demonstrated in Fig. 3. This pumping wavelength is very close to that of widely commercially available 980 nm laser diodes and has the potential to furnish lasing emission wavelengths at 1537 nm or 1556 nm in Er:GaN. In such a context, the pumping mechanism is very similar to the case in the Er doped YAG laser pumped at 980 nm. The disadvantage of employing this quasi-four-level system with a pumping wavelength near 1.0 μm is a large quantum defect (QD) of 0.35, which will translate to a low quantum efficiency as a result of a large amount of heat generation. In comparison, a quasi-three-level system of Er:GaN with resonant pumping is possible with the use of a pumping wavelength at 1514 nm and a lasing emission wavelength at 1537 nm or 1556 nm, providing a very low QD of 0.015 and, hence, very low amount of heat generation.[3] However, this low QD pumping scheme is more difficult to implement due to (a) a small separation between the pumping and lasing wavelengths, (b) less availability of high power LDs operating at 1.514 μm, and (c) less favorable population distribution among different energy levels due to small energy level differences in Er:GaN.[3,4] Both pumping and lasing emission wavelengths in Er:GaN are slightly different from those in Er:YAG[3,4] and also from those in Er doped optical fibers, which typically utilize a pumping wavelength at 980 nm and a lasing wavelength near 1.5 μm.[39,40] Our results presented here clearly demonstrate the importance of determining the detailed energy levels of these manifolds in the $^4I_{11/2}$, $^4I_{13/2}$, and $^4I_{15/2}$ states.

SUMMARY

In summary, Er:GaN epilayers with improved optical qualities over prior attainments have been produced by HVPE. The PL emission spectra resulting from the intra-4f shell transitions from the second excited state ($^4I_{13/2}$) and first excited state ($^4I_{13/2}$) to the ground state ($^4I_{15/2}$) of Er^{3+} ions in GaN have been probed in the 1.0 μm and 1.5 μm regions at room temperature. It was observed that Er:GaN epilayers produced by HVPE in the present work exhibit unprecedented rich spectroscopic features, from which detailed Stark levels in the $^4I_{11/2}$, $^4I_{13/2}$, and $^4I_{15/2}$ states of Er^{3+} ions in GaN were extracted. The results provided an improved agreement with calculation over those previous low temperature PL results measured from MOCVD grown epilayers. The relationship between PL emission intensity (I_{emi}) and excitation laser intensity (I_{exc}) has been measured, revealing a square root power dependence of I_{emi}

on I_{exc}. Polarization-resolved PL emission spectra revealed higher emission intensities at all wavelengths for the TM emission mode than the TE mode, which is consistent with the understanding that this is a direct consequence of the inherent polar material property of wurtzite GaN, giving rise to local fields surrounding the Er site with a net polarization field acting along the c-axis. Furthermore, the energy levels extracted from PL spectra allowed the construction of an energy level diagram involving transitions between Stark levels in the $^4I_{11/2}$, $^4I_{13/2}$, and $^4I_{15/2}$ states of Er:GaN for future HEL applications, which identifies that the optical pumping and lasing emission wavelengths are 1.0 μm and 1.537 (or 1.556) μm for a quasi-four-level lasing system and 1.514 μm and 1.537 (or 1.556) μm for a quasi-three-level lasing system.

ACKNOWLEDGMENTS

DATA AVAILABILITY

The data that support the findings of this study are available from the corresponding author upon reasonable request.

REFERENCES

[1] Y. Kalisky and O. Kalisky, Opt. Eng. **49**, 091003 (2010).

[2] Z. Y. Sun, J. Li, W. P. Zhao, J. Y. Lin, and H. X. Jiang, Appl. Phys. Lett. **109**, 052101 (2016).

[3] Z. Y. Sun, Y. Q. Yan, W. P. Zhao, J. Li, J. Y. Lin, and H. X. Jiang, Appl. Phys. Lett. **112**, 202103 (2018).

[4] Z. Y. Sun, L. C. Tung, W. P. Zhao, J. Li, J. Y. Lin, and H. X. Jiang, Appl. Phys. Lett. **111**, 072109 (2017).

[5] D. W. Jeon, Z. Y. Sun, J. Li, J. Y. Lin, and H. X. Jiang, Opt. Mater. Express **5**, 596 (2015).

[6] P. N. Favennec, H. L'Haridon, M. Salvi, D. Moutonnet, and Y. Le Guillou, Electron. Lett. **25**, 718 (1989).

[7] C. Ugolini, N. Nepal, J. Y. Lin, H. X. Jiang, and J. M. Zavada, Appl. Phys. Lett. **89**, 151903 (2006).

[8] J. Bailey, A. Simpson, and D. Crisp, Publ. Astron. Soc. Pac. **119**, 228 (2007).

[9] J. A. Zuclich, D. J. Lund, and B. E. Stuck, Health Phys. **92**, 15 (2007).

[10] R. Wynne, J. L. Daneu, and T. Y. Fan, Appl. Opt. **38**, 3282 (1999).

[11] H. Furuse, R. Yasuhara, and K. Hiraga, Opt. Mater. Express **4**, 1794 (2014).

[12] W. Xie, S.-C. Tam, H. Yang, J. Gu, G. Zhao, Y.-L. Lam, and W. Tan, Opt. Laser Technol. **31**, 521 (1999).

[13] H. Shibata, Y. Waseda, H. Ohta, K. Kiyomi, K. Shimoyama, K. Fujito, H. Nagaoka, Y. Kagamitani, R. Simura, and T. Fukuda, Mater. Trans. **48**, 2782 (2007).

[14] T. M. Al tahtamouni, M. Stachowicz, J. Li, J. Y. Lin, and H. X. Jiang, Appl. Phys. Lett. **106**, 121106 (2015).

[15] Q. W. Wang, J. Li, J. Y. Lin, and H. X. Jiang, Appl. Phys. Lett. **109**, 152103 (2016).

[16] Q. Wang, R. Hui, R. Dahal, J. Y. Lin, and H. X. Jiang, Appl. Phys. Lett. **97**, 241105 (2010).

[17] J. Heikenfeld, M. Garter, D. S. Lee, R. Birkhahn, and A. J. Steckl, Appl. Phys. Lett. **75**, 1189 (1999).

[18] A. J. Steckl and J. M. Zavada, MRS Bull. **24**, 33 (1999).

[19] S. Kim, S. J. Rhee, X. Li, J. J. Coleman, and S. G. Bishop, Appl. Phys. Lett. **76**, 2403 (2000).

[20] R. Dahal, C. Ugolini, J. Y. Lin, H. X. Jiang, and J. M. Zavada, Appl. Phys. Lett. **97**, 141109 (2010).

[21] V. Dierolf, in *Rare-Earth Doped III-Nitrides for Optoelectronic and Spintronic Applications*, edited by K. O'Donnell and V. Dierolf (Canopus Academic Publishing Ltd.; Springer SBM, 2010), Chap. 8.

[22] A. Braud, in *Rare-Earth Doped III-Nitrides for Optoelectronic and Spintronic Applications*, edited by K. O'Donnell and V. Dierolf (Canopus Academic Publishing Ltd. Springer SBM, 2010), Chap. 9.

[23] R. G. Wilson, R. N. Schwartz, C. R. Abernathy, S. J. Pearton, N. Newman, M. Rubin, T. Fu, and J. M. Zavada, Appl. Phys. Lett. **65**, 992 (1994).

[24] D. K. George, M. D. Hawkins, M. McLaren, H. X. Jiang, J. Y. Lin, J. M. Zavada, and N. Q. Vinh, Appl. Phys. Lett. **107**, 171105 (2015).

[25] Q. Wang, R. Dahal, I.-W. Feng, J. Y. Lin, H. X. Jiang, and R. Hui, Appl. Phys. Lett. **99**, 121106 (2011).

[26] M. Stachowicz, A. Kozanecki, C.-G. Ma, M. G. Brik, J. Y. Lin, H. X. Jiang, and J. M. Zavada, Opt. Mater. **37**, 165 (2014).

[27] I. W. Feng, X. K. Cao, J. Li, J. Y. Lin, H. X. Jiang, N. Sawaki, Y. Honda, T. Tanikawa, and J. M. Zavada, Appl. Phys. Lett. **98**, 081102 (2011).

[28] T. M. Al tahtamouni, X. Z. Du, J. Y. Lin, and H. X. Jiang, Opt. Materi. Express **5**, 648 (2015).

[29] I. W. Feng, J. Li, J. Y. Lin, H. X. Jiang, and J. M. Zavada, Opt. Mater. Express **2**, 1095 (2012).

[30] J. M. Zavada, N. Nepal, C. Ugolini, J. Y. Lin, H. X. Jiang *et al.*, Appl. Phys. Lett. **91**, 054106 (2007).

[31] T. M. Al tahtamouni, X. Z. Du, J. Li, J. Y. Lin, and H. X. Jiang, Opt. Mater. Express **5**, 274 (2015).

[32] S. Alajlouni, Z. Y. Sun, J. Li, J. M. Zavada, J. Y. Lin, and H. X. Jiang, Appl. Phys. Lett. **105**, 081104 (2014).

[33] I. W. Feng, L. Jing, J. Y. Lin, H. X. Jiang, and J. Zavada, Appl. Opt. **52**(6), 1132 (2013).

[34] I. Izeddin, T. Gregorkiewicz, D. S. Lee, and A. J. Steckl, Superlattices Microstruct. **36**, 701 (2004).

[35] J. Zhou, W. Zhang, J. Li, B. Jiang, W. Liu, and Y. Pan, Ceram. Int. **36**, 193 (2010).

[36] W. F. Zhang, M. S. Zhang, Z. Yin, and Q. Chen, Appl. Phys. B **70**, 261 (2000).

[37] L. Skuja, K. Tanimura, and N. Itoh, "Correlation between the radiation-induced intrinsic 4.8 eV optical absorption and 1.9 eV photoluminescence bands in glassy SiO$_2$," J. Appl. Phys. **80**, 3518 (1996).

[38] Y. Q. Yan, Z. Y. Sun, W. P. Zhao, J. Li, J. Y. Lin, and H. X. Jiang, Appl. Phys. Express **12**, 075505 (2019).

[39] G. Sobon, J. Sotor, J. Jagiello, R. Kozinski, M. Zdrojek, M. Holdynski, P. Paletko, J. Boguslawski, L. Lipinska, and K. M. Abramski, Opt. Express **20**, 19463 (2012).

[40] J. Sotor, G. Sobon, W. Macherzynski, P. Paletko, K. Grodecki, and K. M. Abramski, Opt. Mater. Express **4**, 1 (2014).